Applied Energy 400 (2025) 126570

Contents lists available at ScienceDirect

Applied Energy

journal homepage: www.elsevier.com/locate/apenergy

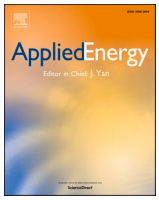

Towards integrated photovoltaic applications: Lightweight silicon heterojunction solar modules with different encapsulation materials and their damp heat stability

Kai Zhang [a,b,*], Andreas Lambertz [a], Krzysztof Dzięcioł [c], Karsten Bittkau [a], Rongda Zhang [a], Yanxin Liu [a,b], Andreas Gerber [a], Henrike Gattermann [a], Rüdiger-A. Eichel [c,d,e], Uwe Rau [a,b], Christoph J. Brabec [a,f], Kaining Ding [a,*]

[a] IMD-3 Photovoltaics, Forschungszentrum Jülich GmbH, 52428 Jülich, Germany
[b] Jülich Aachen Research Alliance (JARA-Energy) and Faculty of Electrical Engineering and Information Technology, RWTH Aachen University, 52074 Aachen, Germany
[c] Institute of Energy Technologies (IET-1: Fundamental Electrochemistry), Forschungszentrum Jülich GmbH, 52428 Jülich, Germany
[d] Faculty of Mechanical Engineering, RWTH Aachen University, 52062 Aachen, Germany
[e] Institute of Physical Chemistry, RWTH Aachen University, 52074 Aachen, Germany
[f] Institute of Materials for Electronics and Energy Technology (i-MEET), Friedrich-Alexander University Erlangen-Nürnberg, Erlangen, Germany

HIGHLIGHTS

- Lightweight SHJ solar modules with a low area density while preserving high power density were fabricated.
- The efficiency loss in lightweight modules after DH test varied significantly, depending on the encapsulation materials.
- The TPO encapsulants show promising compatibility for encapsulating SHJ solar cells.
- An optimized damp heat-stable lightweight SHJ solar module has been successfully developed.
- Provide insights into the degradation mechanism of lightweight SHJ solar modules with different encapsulation materials.

ARTICLE INFO

Keywords:
Silicon heterojunction (SHJ)
Lightweight solar module
Encapsulation
Damp heat-induced degradation (DHID)
Reliability

ABSTRACT

Lightweight photovoltaic (PV) modules are able to open up vast new scenarios for PV applications, like building-integrated PV (BIPV) and vehicle-integrated PV (VIPV). Silicon heterojunction (SHJ) solar cells have been recognized as one of the most advanced technologies for improving solar power generation. However, SHJ solar cells are inherently susceptible to damp heat-induced degradation (DHID), which is a critical concern for their application. In this study, lightweight SHJ mini-modules with a low area density (~ 2 kg/m^2) while preserving high power density (~ 70 W/kg) were fabricated using SHJ solar cells with different encapsulation materials and architectures. A comprehensive analysis of the module degradation was carried out, focusing on the optical and electrical properties of the modules and the chemical properties of the encapsulants after 1000 h of accelerated damp heat (DH) aging test. The efficiency loss in lightweight SHJ solar modules after DH test varied significantly, ranging from 3.22 %$_{rel}$ to 54.06 %$_{rel}$, depending strongly on the encapsulation materials. The increase in series resistance (R_s) was generally the dominant cause of module efficiency degradation. An optimized damp heat-stable lightweight SHJ module was successfully fabricated, with only 0.47 %$_{rel}$ efficiency degradation after 1000 h of the DH test. Its stability is almost the same as that of the glass/back sheet module. The comparative study and comprehensive investigation provide insights into the DHID behavior of lightweight SHJ solar modules with different encapsulation materials, contributing to the development of lightweight SHJ solar modules with high DH stability for industrialized mass production.

* Corresponding authors at: Forschungszentrum Jülich GmbH, 52428 Jülich, Germany.
E-mail address: k.zhang@fz-juelich.de (K. Zhang).

https://doi.org/10.1016/j.apenergy.2025.126570
Received 4 March 2025; Received in revised form 7 June 2025; Accepted 31 July 2025
Available online 6 August 2025

1. Introduction

Conventional crystalline silicon (c-Si) photovoltaic (PV) modules usually consist of a superstrate solar glass covering, silicon solar cells, two layers of polymeric encapsulant (one on the front of the solar cell and another on the rear of the solar cell), a substrate polymeric back sheet or glass, an aluminum frame, a junction box, and other materials such as ribbons [1,2]. This architecture was developed in the late 1970s, and has not changed significantly since then. The glass/back sheet module normally has an area density in the range of 12–16 kg/m^2, and the glass/glass module has an area density in the range of 14–20 kg/m^2 [3–5], which poses limitations for application scenarios, such as roofs with low load tolerances and integrated applications. For these areas of application, properties such as lightweight and flexibility are becoming increasingly significant for the design of PV modules. Lightweight PV modules are not only applicable to the ground installation, but also opens up the scenarios like the building-integrated PV (BIPV) and the vehicle-integrated PV (VIPV) [6]. In recent years, researchers have been working on the development of lightweight PV modules by substituting the cover glass with ultra-thin glass [7] or even lighter materials such as polymer foils [3,8–10].

Silicon heterojunction (SHJ) solar cells are recognized as one of the most advanced technologies for improving solar power generation [11,12]. It can achieve a high power conversion efficiency (PCE) owing to its excellent surface passivation to minimize surface recombination, resulting in a higher open-circuit voltage (V_{OC}) and fill factor (*FF*) compared to other c-Si-based cell technologies, such as the aluminum back-surface field (Al-BSF) cell and passivated emitter rear contact (PERC) cell. The world record highest PCE of 27.08 % for a 210 × 105 mm^2 both sides contacted SHJ cell was reported by Trinasolar in December 2024 [13]. In addition, SHJ solar cells are highly compatible with bifacial PV module designs and integrated PV applications owing to their symmetric architecture. Therefore, a combination of SHJ solar cell technology with a lightweight module configuration would be a good attempt. The concept of the lightweight module is to replace the conventional glass cover with a polymeric sheet. Since this sheet is placed on the front side, it must be transparent to sunlight. Ethylene tetrafluoroethylene (ETFE) has been used as the front sheet owing to its high transparency and stability [3,4]. Thus, the module has a front sheet/back sheet structure. Moreover, a metal frame is not required either. This reduces the module area density to approximately 1.75 kg/m^2.

However, several challenges are associated with the development and deployment of lightweight SHJ solar modules. At the cell level, in general, SHJ solar cells are more sensitive to moisture than other solar cell technologies, such as PERC cell technology [14], due to the hydrophilic nature of the deposited amorphous silicon layers. Different transparent-conductive oxide (TCO), such as indium tin oxide (ITO) and aluminum-doped zinc oxide (AZO), have varying resistance to damp heat (DH) [15]. The SHJ solar cell is degraded by moisture ingress with increasing temperature, causing damp heat-induced degradation (DHID), which decreases the module power output in the long run. At the module level, a reliable encapsulation solution is only available for glass/glass structures, and it is not yet ready for front sheet/back sheet structures. Naturally, the glass facing the front acts as the first protection of the glass module. However, the lightweight module architecture faces a critical challenge of a higher water-vapor transmission rate (WVTR) than conventional glass/back sheet or glass/glass encapsulated modules. Therefore, the lightweight module is literally more susceptible to DHID than the glass module. Thus, the degree of protection required from the front and back sheets also increases, which means a lower permeability of the components is required. These components, particularly the polymeric elements of PV modules, play a vital role in the durability and reliability of these devices [2,16]. The appropriate choice of encapsulants with cell technology is critical to the life span of PV modules. Therefore, introducing new materials and material combinations should be preceded by a thorough testing of each new combination [17].

Ethylene-vinyl acetate (EVA) copolymer has been the dominant module encapsulant choice for decades because of its advantages, such as high transmittance, good adhesion to glass, favorable mechanical properties, and low cost [1,18]. Although EVA is the most widely used encapsulant for PV modules, it has some drawbacks, such as peroxide-induced cross-linking and the production of corrosive acetic acid in the presence of moisture and other environmental stressors, which can lead to the corrosion of metal grids and other components of PV modules [2,19], resulting in decreased reliability of PV modules. In recent years, different types of next-generation encapsulant foils have been introduced and have attracted increasing attention in the market. These newer encapsulants can be categorized as polyolefin elastomer (POE) encapsulants and thermoplastic polyolefin (TPO) encapsulants [40,41], both of which consist of a polyethylene backbone with different side groups. The main advantage of these encapsulants is the replacement of the vinyl acetate side groups of EVA, by acrylates, acrylic acids or n-alkanes; with no formation of acid consequently. Similar to EVA, POE contains cross-linking agents (peroxide), and therefore has a similar lamination process as EVA. TPO is a thermoplastic elastomer that exploits thermo-reversible physical cross-linking, such as ion bonds, hydrogen bonds or via crystallites [17], showing potential in recycling of solar modules. Moreover, TPO is free of peroxide, which can potentially corrode solar cells. EPE (EVA/POE/EVA), which is a co-extruded of EVA and POE that combines the advantages of EVA with low-cost and POE with better material properties. In general, these new types of encapsulants, such as TPO and POE, have lower WVTR than EVA and are suitable for moisture-sensitive advanced cell and module technologies [17,20]. However, few studies have reported the selection of encapsulants that are compatible with the SHJ cell technology within a lightweight module architecture [21,22].

During long-term operation in the field, the modules will suffer from environmental and weather impacts, such as moisture ingression, elevated temperature, and ultraviolet (UV) radiation. These environmental factors would lead to performance degradation of solar modules. Encapsulation materials play an important role in module reliability because the most prominent module failure mechanisms are linked to the polymeric encapsulation materials used. Polymeric encapsulants and front or back sheets are important for PV modules because of their various functions [1,2,23]. However, these polymeric components are not perfectly air/water-tight and are prone to permeation of gases, including moisture, oxygen, and other gaseous species from ambient surroundings [19]. Moisture ingress usually occurs through polymeric materials, module edges, and voids created by manufacturing, handling, and climatic stressors [24–29]. Once water penetrates the solar module, the accumulated moisture within the module in the presence of other climatic stressors can lead to all forms of degradation modes in the components of PV modules [30,31]. Moisture ingress at elevated temperatures leads to the formation of acetic acid within the EVA encapsulant. Acetic acid accumulation in solar modules is a major precursor for interconnect corrosion, which usually occurs around cell interconnect ribbons and cell metallization in modules [2,32–34]. According to Peshek et al. [35], the routes of corrosion are dominated by moisture ingress from the perimeter to the interior of the module. Discoloration can also result from moisture ingress in PV modules [25]. Particulate water trapped within the encapsulants acts as an optical barrier, increasing absorption losses, which has a significant effect on the quantum efficiency of the modules [35–37]. Additionally, moisture ingress induces adhesion loss and creates voids which serve as a suitable reservoir for moisture and gas accumulation [38] in the encapsulants and back sheets, thereby predisposing all components of the PV module to corrosion [38–41] and therefore may result in power loss [41,42]. The loss of adhesion between solar cells, encapsulants, glass, and other active layers due to environmental, climatic, and/or artificial mechanical stressors results in delamination [18,24]. Delamination and discoloration cause optical performance losses [27,43].

UV radiation has been identified as another critical factor for module degradation and its lifetime by many research groups. UV radiation can trigger chemical reactions and degradation processes of polymers in solar modules, which changes the primary structure of the polymer, causing crosslinking or the breaking of the chains, and other chemical alterations [1]. Typical defect, such as encapsulant discoloration, like EVA yellowing, is caused by photo-oxidation due to UV radiation. Acetic acid and aldehyde can be formed due to UV radiation and temperature [1]. It has also been reported that encapsulants are susceptible to losing adhesion under UV irradiation [44,45]. In addition, from the perspective of SHJ solar cells, the silicon-hydrogen (Si—H) bond can be broken by high-energy UV photons, consequently leading to the deterioration of the chemical passivation properties of SHJ solar cells [46]. Overall, the degradation of polymer encapsulants and SHJ solar cells due to UV radiation has a synergistic degradation effect on lightweight solar modules. However, UV-induced degradation (UVID) is not the main focus of this study. Further insights into the mechanism of UVID behavior on lightweight SHJ solar modules will be comprehensively investigated in our future work.

Overall, the damp heat stability is a critical challenge for lightweight SHJ solar modules. Addressing these challenges is crucial for the development and commercialization of lightweight SHJ solar modules to ensure that they meet the performance and durability standards required for diverse applications.

This study focuses on the development of SHJ solar cell-based lightweight modules that are resistant to damp heat impact. The performance and reliability of various combinations of encapsulants/front sheets with SHJ solar cells in a lightweight configuration under damp heat conditions were analyzed comprehensively. We investigated the impact of humidity and temperature on the optical and electrical behaviors of lightweight PV modules. The degradation mechanism related to each failure mode was analyzed accordingly.

2. Experiment and method

2.1. Lightweight module design

Fig. 1 shows the schematic cross-section of the lightweight SHJ solar module, which has a similar sandwich structure compared to conventional glass/back sheet modules. However, the front glass is replaced by a polymer front sheet, and the edge sealant material is added between the front sheet and back sheet.

Single cell mini-module samples measuring 210 mm × 210 mm were prepared using M2+ (156.75 mm × 156.75 mm) size bifacial monocrystalline busbar-free n-type rear-junction SHJ solar cells. The cells are connected using multiwire interconnection technology, which is composed of 18 coated copper wires with polyolefin (PO) as a carrier foil. This foil is in direct contact with the cell and sits between the cell and the encapsulant. Sn-Pb-coated Cu-ribbons were used as connectors. For the fabrication of the lightweight solar modules, four different front sheet materials, ethylene tetrafluoroethylene (ETFE), polyvinyl fluoride (PVF), polyethylene terephthalate (PET), and polyvinyl fluoride/polyethylene terephthalate (PVF/PET) laminated foil were used. The specifications of the front sheets are listed in Table S1 of the Supplementary Information. The following encapsulants were used, thermoplastic polyolefin (TPO), thermoplastic polyurethane (TPU), transparent ethylene-vinyl acetate [EVA(T)], white ethylene-vinyl acetate [EVA(W)], polyolefin elastomer (POE) [POE—S: POE with UV-transmitting property & POE-UV: POE with UV-blocking property], EVA/POE/EVA (EPE), UV-downshifting EVA (DS-EVA), and UV-downshifting EPE (DS-EPE). These encapsulants are categorized into three groups based on their light transmission to UV light (280–400 nm). TPO, TPU, and POE-UV are UV-blocking encapsulants. EPE, POE—S, and EVA(T) are UV-transmitting encapsulants. DS-EVA and DS-EPE are UV-downshifting encapsulants that can convert UV light to blue light. The specifications of the encapsulants are listed in Table S2. A polyolefin-based foil with aluminum as the interlayer was used as the back sheet which is donated as Al-bs in following. The specifications of the back sheet are listed in Table S1. The edges of the modules were sealed using polyisobutylene (PIB) tape. The specifications of the edge sealant are listed in Table S3. The overall thickness of the modules was less than 2 mm. Table 1 lists the configurations of the test modules with different encapsulants. Table 2 lists the configurations of the test modules with different front sheets. The TPO was used as encapsulant in this case as it shows the most stable performance in DH test, see Section 3.1. The glass/glass and glass/back sheet module samples were used as references for comparison.

2.2. Module fabrication process

The modules were fabricated by a typical vacuum lamination process using a laminator from *SM Innotech*. The parameters of the lamination process for each sample type are listed in Table S4. Two identical modules were fabricated for each configuration. The cells used for modules fabrication have the same performances.

2.3. Accelerated DH aging tests

Accelerated DH aging tests were performed at 85 °C and 85 % relative humidity (RH) in a *ESPEC* climate chamber for accumulated 1000 h according to the IEC 61215 protocol [47]. The modules were placed vertically in a holder in a climate chamber, as shown in Fig. S1.

Table 1
Configurations of the test modules with different encapsulants.

Front sheet	Encapsulants (front/rear)	Back sheet
ETFE	TPO	Al-bs
	TPU	
	POE-UV	
	EPE	
	EVA(T)/EVA(W)*	
	POE-S	
	DS-EVA	
	DS-EPE	

Abbreviations: EVA, ethylene-vinyl acetate; POE, polyolefin elastomer; TPO, thermoplastic polyolefin; TPU, thermoplastic polyurethane; EVA(T), transparent EVA; EVA(W), white EVA; EPE, EVA/POE/EVA; DS-EVA, UV-downshifting EVA; DS-EPE, UV-downshifting EPE; ETFE, ethylene tetrafluoroethylene; Al-bs, polyolefin-based aluminum back sheet. * Transparent EVA was used on the front side of the cell and white EVA was used on the rear side of the cell.

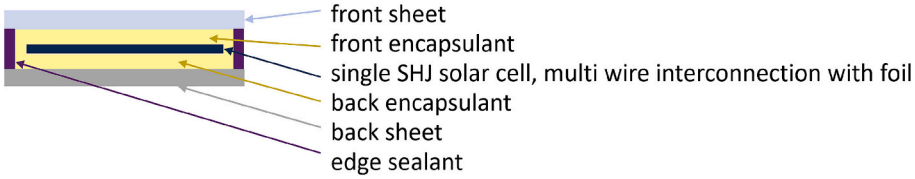

Fig. 1. Schematic of the lightweight SHJ solar module.

Table 2
Configurations of the test modules with different front sheets.

Front sheets	Encapsulants (front/rear)	Back sheets
ETFE	TPO	Al-bs
PVF		Al-bs
PET1 (PVF/PET)		Al-bs
PET2		Al-bs
glass		Al-bs
glass		glass

Abbreviations: ETFE, ethylene tetrafluoroethylene; TPO, thermoplastic polyolefin; Al-bs, polyolefin-based aluminum back sheet; PVF, polyvinyl fluoride; PET, polyethylene terephthalate.

2.4. Characterization techniques

The analysis of the performance and performance degradation mechanism of the modules due to the DH effect was carried out based on the following characterization methods. The current-voltage (*I-V*) characterization under standard test conditions (STC: AM1.5 G, 25 °C, 1000 W/m^2), electroluminescence (EL) imaging and external quantum efficiency (*EQE*) of the modules were measured by using a LOANA solar cell and module analysis system from *PV-Tools*. X-ray computed tomography (XCT) images were taken using a Zeiss Xradia Versa 620, voxel size is 740 nm, X-ray tube voltage is 100 kV. The total spectral transmittance (*T*) and reflectance (*R*) were measured from 300 nm to 1200 nm in 5 nm steps using a UV–vis-NIR spectrophotometer with an integrating sphere (*Perkin Elmer*, LAMBDA 950). Raman spectra of the polymer encapsulant foils were performed from 0 to 4000 cm^{-1} using *inVia* confocal Raman microscope with 10 mW power, 50× magnification, 532 nm excitation laser source, 10 s of exposure time.

3. Results and discussion

3.1. Damp heat stability of lightweight modules with different encapsulants

3.1.1. I-V characteristics

Fig. 2 shows the development of the electrical properties of the modules encapsulated with different encapsulants over a regular time interval (200h) during the DH test. The variance in efficiency for modules with the same configurations is shown in Fig. S2. It was found that after 1000 h of DH test, the module encapsulated with EPE had the largest efficiency degradation of 54.06 %$_{rel}$, whereas the module encapsulated with TPO had the lowest efficiency degradation of 3.22 %$_{rel}$. The relative efficiency degradation (D_η^{rel}) was defined and calculated by eq. (1). A efficiency/power loss of less than 5 %$_{rel}$ is required for c-Si PV modules by IEC 61215 [47]. However, there is no specific norm for lightweight glass-free modules. It is easy to see that the efficiency degradation of modules is mainly due to the decrease in *FF*. The *FF* loss was mainly attributed to the increase in series resistance (R_s), as the pseudo fill factor (p*FF*) was almost constant during DH test. Among all the modules, the EPE module demonstrates a dramatic increase in R_s, which was assumed to be attributed to the electrical contact problems that probably arise from two parts: the contact between the fingers and wires, and the contact between the wires and ribbons [48]. Additionally, a very large increase in R_s (typical values are from 0.8 to 10 Ωcm^2) would lead to a decrease in short-circuit current density (J_{sc}) [49,50], which was also observed in the EPE module. In addition, the DS-EPE module also demonstrated a significant increase in R_s.

$$D_\eta^{rel}(\%) = \left(1 - \frac{\eta_{DH1000h}}{\eta_{DH0h}}\right) \times 100 \quad (1)$$

Except for a slight reduction in V_{oc} for the EVA and POE-S modules, the V_{oc} of all other modules remained almost constant with DH time. The reduction in V_{oc} can be explained by the increase in the saturation current density (J_{01}) according to the relationship between V_{oc} and J_{01} [51]:

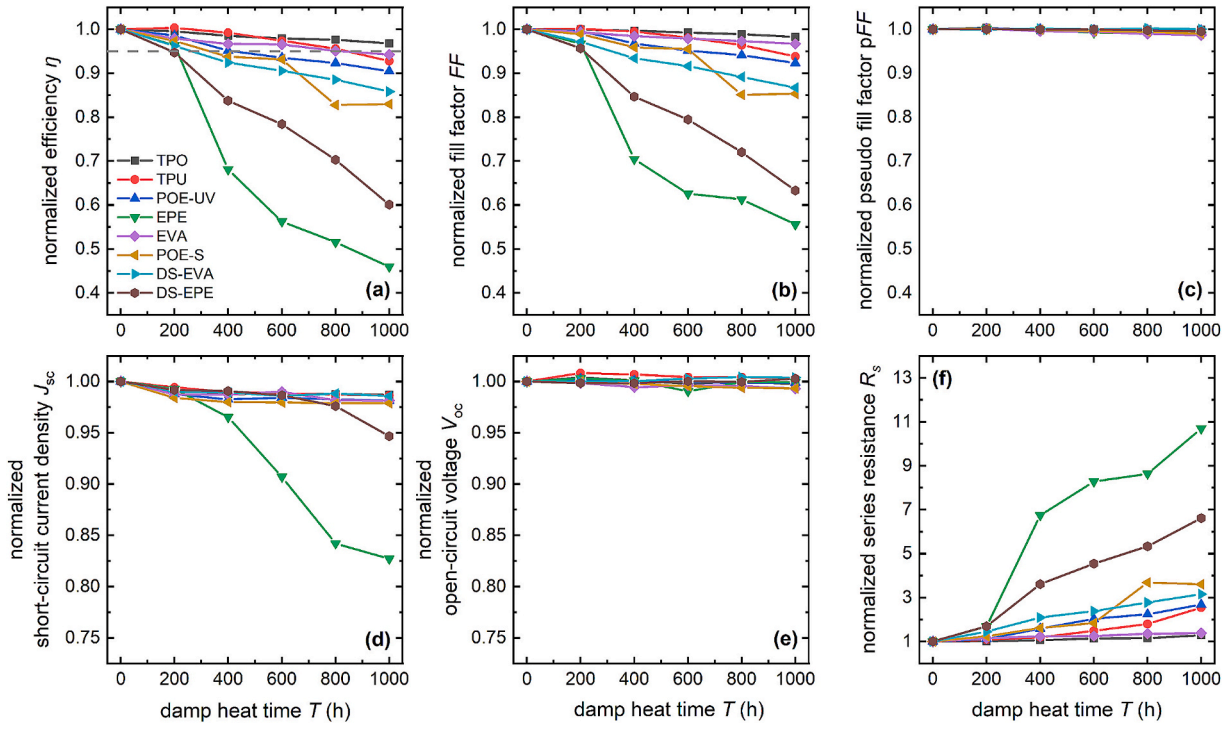

Fig. 2. Normalized values of (a) efficiency (η), (b) fill factor (*FF*), (c) pseudo fill factor (p*FF*), (d) short-circuit current density (J_{sc}), (e) open-circuit voltage (V_{oc}), and (f) series resistance (R_s) as a function of damp heat time for modules encapsulated with different encapsulants.

$$V_{oc} = \frac{kT}{q}\ln\left(\frac{J_{sc}}{J_{01}} + 1\right) \quad (2)$$

From the dark *I-V* curves of the modules, as shown in Fig. S3, we observed a slight increase in J_{01} for the EVA and POE-S modules. The increase in J_{01}, which is associated with the recombination processes occurring in the surface and bulk of the solar cell [49,52], is most visible in the medium- and high-voltage regions of the dark *I-V*, which is consistent with our observations. This indicates that the passivation layers of the SHJ solar cells in the EVA and POE-S modules were slightly degraded owing to the damp heat effect.

TPO-encapsulated module exhibited the most stable performance with slower degradation kinetics during DH aging compared to the other investigated encapsulants. From the perspective of material properties, TPO exhibits the highest degree of crystallinity compared to POE and EVA, as reported by Oreski et al. [17,20]. In terms of thermo-mechanical stability, TPO exhibits the most stable behavior due to its high melting temperature, resulting in low thermal expansion [17,20]. Studies also show that crystallinity has a dominant effect on the thermo-mechanical behavior of encapsulants [17], which explains why TPO exhibits better thermo-mechanical stability. In addition, TPO encapsulants have good hydrolytic stability due to their specific low chemical polarity and high crystallinity [20]. The TPO and ETFE laminated film exhibits the low WVTR as shown in Table S2, thus could provide better resistance to the moisture ingress compared with other investigated encapsulants.

Moisture ingress can trigger DH-induced defects. However, from the WVTR results shown in Table S2, there is no direct relationship between the WVTR of encapsulation materials and the module efficiency degradation. The degradation of the lightweight SHJ solar modules is the consequence of the synergistic effect of moisture ingress and the properties of the polymer materials. These properties depend not only on hydrolytic properties, but also on factors such as chemical composition and thermo-mechanical properties.

3.1.2. *EL imaging*

Fig. 3 shows the EL images taken at low current (~ 0.5 A) injection conditions with an exposure time of 3 s for all modules before and after 1000 h of DH test. EPE and DS-EPE modules showed significant defects in the EL images, while the EPE module showed very specific defects in the EL images. Looking at the EL images of the EPE module shown in Fig. 3(d), a dark band which is marked by a red rectangular shape, was found on the top of the EPE module after 1000 h of the DH test, probably caused by the contact failure between the wires and ribbons. This defect was also observed in the DS-EPE module, as shown in Fig. 3(h). To investigate this issue further, a re-soldering process was performed on another EPE module with the same configuration, which underwent the same DH test batch and showed identical defects to those observed in the EPE module shown here. The EL images and *I-V* characteristics were measured again after each re-soldering process, as shown in Fig. S4. After re-soldering the wires with ribbons, the efficiency of the module was recovered accordingly. The R_s was reduced and J_{sc} also improved. Additionally, looking at the light *I-V* curves shown in Fig. S4(b), the current in the reverse-bias voltage can reach saturation, which indicates that the decrease in J_{sc} is due to the increase in R_s rather than being influenced by optical degradation. The significant increase in R_s affected the transport of the carriers resulting in the decrease in J_{sc}. Moreover, the dark band in the EL was eliminated. This indicates that the dark band in the EL of the EPE and DS-EPE modules were caused by the detachment of the contacts between the wires and ribbons due to the solder joint failure, resulting in a significant increase in R_s. Fig. S4(c) shows a schematic of the solder joint failure between wire and ribbon. A slight bending of the module edges was observed because of the elevated temperature during the DH process, as the lightweight module was not as rigid as the glass module. The modules were placed vertically in a holder within the climate chamber, and the edges in contact with the holder were easily softened by the high temperature. This increases the risk of solder joint deterioration, resulting in wire detachment from the ribbon.

In addition to this dark band defect, we also observed another defect in the EL of the EPE module. Some bright and dark intersection regions can be seen in the EL image of the EPE module, as shown in Fig. 3(d). In general, contact failure could be induced by chemical corrosion, such as acetic acid formation, or thermal stress [53]. We suspected that this defect was probably caused by contact failure between the fingers and wires due to thermal stress, rather than corrosion of the metallization. Corrosion of metal contacts is mostly prominent when using EVA encapsulants, which form acetic acid [17]. Acetic acid formation can also occur with EPE encapsulants. However, there is no indication of increased acetic acid in the EPE module after 1000 h of the DH test from Raman spectroscopy analysis in Section 3.1.5. The cell is additionally protected by a polyolefin interconnection foil, which is in direct contact with the cell and sits between the cell and encapsulant. The moisture/acetic acid would degrade the surface of the cell (e.g. ITO) earlier than corrode contacts [54]. The defect is supposed to expand due to the diffusion of moisture/acetic acid. However, the expansion of such defects was not observed in the evolution of the EL images at 200-h intervals as shown in Fig. S6. It is identified that the defect occurred between 200 and 400 h, and that the defect was exacerbated by prolonging the DH aging time. Meanwhile, the efficiency degradation shows a significant drop between 200 and 400 h. Therefore, we can temporarily conclude that this bright and dark intersection defect was primarily caused by contact failure due to thermal stress. A detailed microscopic analysis of this defect was carried out using XCT as described in Section 3.1.3.

In DS-EVA module, defects in EL image are also likely to be caused by

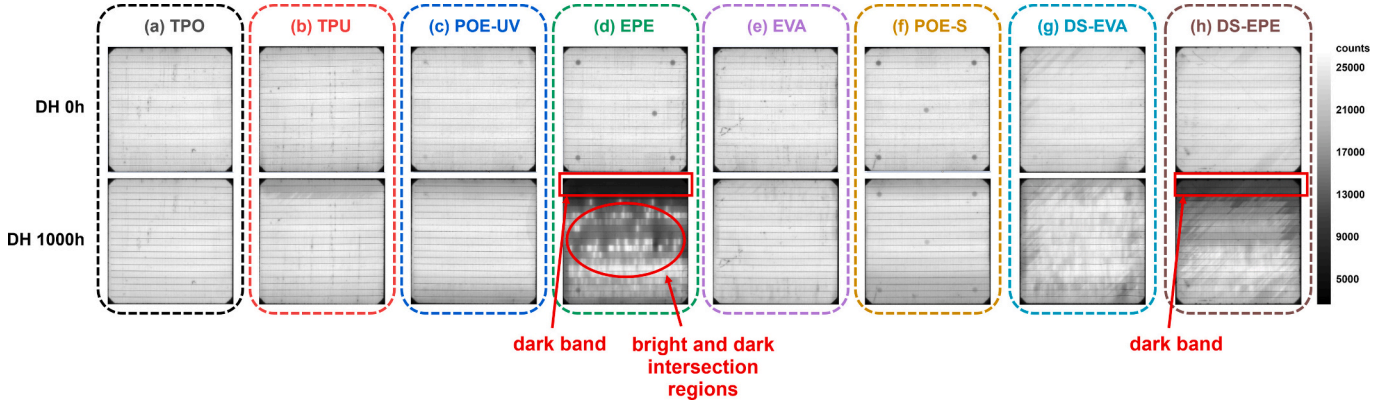

Fig. 3. EL images of the modules encapsulated with different encapsulants (a) TPO, (b) TPU, (c) POE-UV, (d) EPE, (e) EVA, (f) POE—S, (g) DS-EVA and (h) DS-EPE before and after 1000 h of the DH test. EL images of all modules with their individual scales are shown in Fig. S5.

the interconnection issue between the fingers and interconnection wires. Additionally, an edge defect [55] due to the moisture ingress from the module edges was also observed in DS-EVA module. The bands with lower luminescence were also found in EL images in TPU, POE-UV and POE-S modules and are also likely to be caused by the degradation of the contact between the wires and ribbons. For the rest of the modules, we did not observe any obvious defects in the EL images.

3.1.3. X-ray computed tomography

In order to have a deep understanding of the bright and dark intersection regions defect in the EL of the EPE module. XCT was used for in-depth investigation. A strip of the degraded EPE module was selected and cut out for X-ray scanning. The area selected for X-ray scanning is marked by a blue rectangle in Fig. 4(a) and is divided into eight regions of interest (ROI) from ROI1 to ROI8. Two areas (ROI1-ROI2 and ROI7-ROI8), which contained two distinct EL intensities, were selected for further XCT scanning analysis. From the reconstructed images in Fig. 4 (b), we can clearly see the intact interaction of the finger and wire in the ROI1-ROI2 area. However, we found the finger breakage in the ROI7-ROI8 area as shown in Fig. 4(c), which was caused by the detachment of the wires, resulting in contact failure between the fingers and wires. It is reported that the thermal loading creates deformation in copper wires and this deformation is stored in the copper wires as strain energy. As the strain energy accumulates with increased thermal loading, this eventually results in fatigue failure [56,57]. As discussed in Section 3.1.2, we believed that the decrease in conductivity between the wires and fingers was caused by the wires detaching from the fingers due to thermal stress during the DH process. This was confirmed by the results of the XCT analysis. In a solar module, each layer has a different coefficient of thermal expansion (CTE), and these differences can create thermal stresses during temperature changes [56]. Differential expansion and contraction of materials with varying CTE can lead to cracking, solder joint fatigue, and interface delamination, thus affecting the long-term reliability of the module. However, the investigation of degradation mechanism of the thermo-mechanical properties of the module is beyond the scope of this work. This will be further investigated in our future work.

The above analyses from EL imaging and XCT confirm that the increase in R_s in the EPE module is primarily caused by solder joint failures between the wires and ribbons, and interconnection failures between the fingers and wires.

3.1.4. Visual inspection and optical properties analyses

In addition to analyzing the electrical properties of the modules before and after the DH test, a visual inspection of the modules was carried out to identify the defects such as cracks, discoloration, delamination, and soldering defects. Visual images of all types of modules before and after the DH test are shown in Fig. S7. From the visual inspection of the module, a slight bending at the edges of the modules was observed. Because the modules were placed vertically in a holder in the climate chamber, the edges softened owing to the elevated temperature. Additionally, an obvious yellowing effect was observed in the EVA module, particularly at the edges of the module (over the white back sheet), as shown in Fig. 5(a). Several investigations have shown that EVA discoloration (yellowing or browning) results primarily from the formation of polyconjugated C═C bonds (polyenes) by multistep deacetylation and from the presence of 1,3-unsaturated carbonyl groups due to thermal oxidation, and is enhanced by increased UV radiation [1,23,58]. Another source for discoloration is the production of chromophores and luminophores from additives in encapsulant and not from the encapsulant itself [1]. In our case, a single DH process without UV radiation resulted in a light yellowing effect.

To identify the changes in the optical properties of the encapsulants, the modules were dismantled to obtain aged encapsulants. The transmittance and reflectance spectra of the aged encapsulants were measured and compared with those of unaged encapsulants. The preparation process of unaged encapsulant samples is provided in the Supplementary Information. The EVA(T) encapsulant exhibited a minor reduction in transmittance in the 300–400 nm wavelength range, whereas the reflectance remained constant before and after DH, as shown in Fig. 5(b). This indicates that the optical loss from the encapsulant was mainly due to the increased light absorption. Therefore, we observed only a 0.93 $\%_{rel}$ reduction in the photocurrent for the EVA module according to the integrated current calculated from the *EQE* measurements (in Section 3.1.6). This indicates that the negligible reduction in photocurrent was caused by the yellowing effect of the EVA modules. As for the rest of the modules, we did not observe any obvious discoloration and other defects.

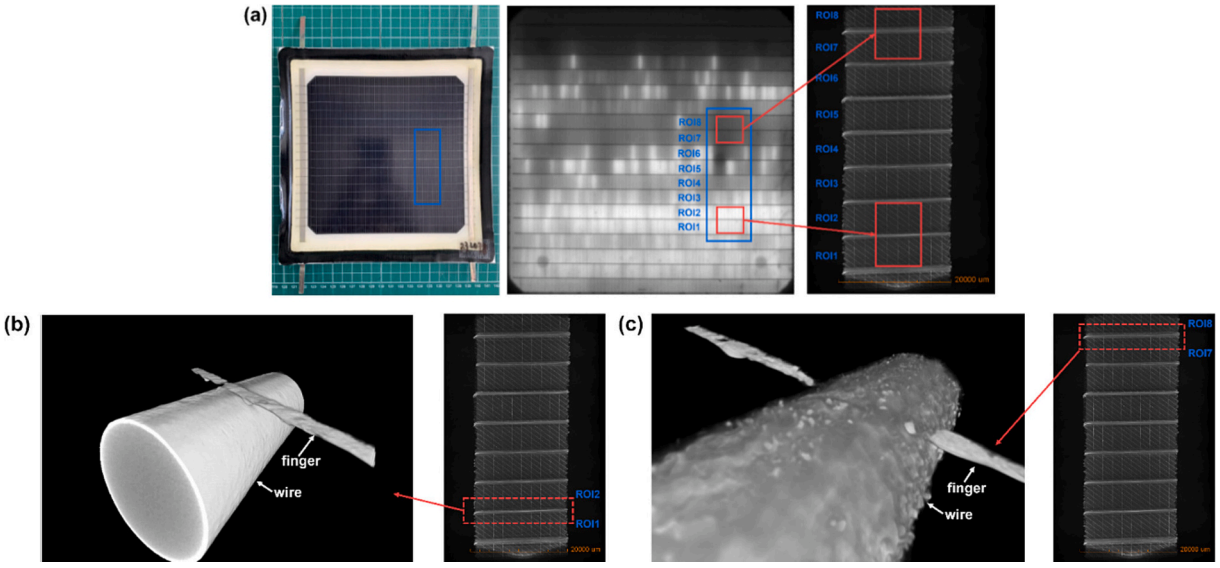

Fig. 4. X-ray computed tomography (XCT) of the degraded EPE module: (a) X-ray scanning of two areas, ROI1-ROI2 and ROI7-ROI8, which contain two distinct EL intensities. (b) Reconstructed image showing intact interaction of the finger with the wire in the ROI1-ROI2 area. (c) Reconstructed image showing finger breakage in the ROI7-ROI8 area. The XCT images were taken by Zeiss Xradia Versa 620, voxel size is 740 nm, X-ray tube voltage is 100 kV, exposure time per projection is 15 s, and the number of projections is 1200.

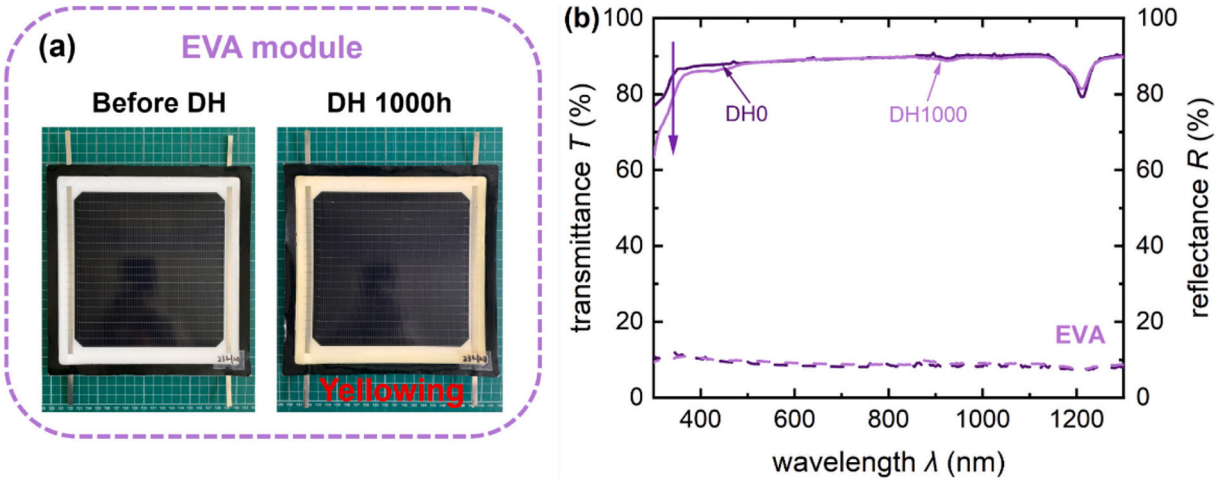

Fig. 5. (a) Visual images of EVA-encapsulated modules before and after 1000 h of the DH test. (b) Transmittance (solid line) and reflectance (dash line) of EVA encapsulant foil before and after 1000 h of the DH test.

3.1.5. *Raman spectroscopy analysis*

Raman spectroscopy analyses were performed on the encapsulants samples before and after 1000 h of the DH test to further check the polymer encapsulants degradation process. The aged encapsulant samples were obtained from the dismantled modules after 1000 h of DH aging test. The encapsulant sample was positioned at the center and above the cell. The details of the preparation of the unaged encapsulant samples are provided in the Supplementary Information.

Fig. 6 shows the Raman raw spectra of the different encapsulants before and after 1000 h of the DH tests. This is mainly an investigation of the fluorescence background [59,60]. A significant increase in the fluorescence background was observed in the DS-EPE sample. TPU showed the least increase in the fluorescence background, as shown in Fig. 6(c). The intensity of the fluorescence background, which is related to the formation of chromophore groups (containing polyconjugated C═C bonds), is an indicator of polymer aging. The chromophore groups can exhibit strong fluorescence and are one reason for the yellowing of the encapsulant [60].

In addition, the raw Raman spectra of the EVA(T) encapsulants at different locations in the EVA module after 1000 h of DH test were analyzed, as shown in Fig. S8. We obtained EVA(T)-encapsulant samples from three typical positions in the module. Two samples were located on the left edge of the module, over the white back sheet. Two samples were located on the top edge of the module, over the white back sheet. Two samples were located at the center of the module over the cell. Strong fluorescence background in raw Raman spectra (Fig. S8) is observed at the left and top edges of the module. This indicates that the chromophore groups were mainly generated at the edges of the module, resulting in yellowing of the EVA module. These findings confirmed that moisture ingress as the driver of discoloration is more severe at the module edges than at the center of the module.

The normalized Raman spectra are shown in Fig. S9. We did not observe any obvious decrease in the Raman peaks of encapsulants. The EVA encapsulant is most likely to release acetic acid in the presence of moisture, which can lead to the corrosion of metal grids and other components of solar modules, resulting in an increased R_s. However, the normalized Raman spectra show no sign of an increase in the acetate group (OCO, 629 cm^{-1}). This indicates that there is no formation of acetic acid after DH. And no typical corrosion defects were observed in the EL imaging. The increase in R_s is as low as that of the TPO module, which is free of acid formation. Therefore, we conclude that acid corrosion is not the major degradation mechanism for the EVA module in our case. In addition, for other EVA-containing encapsulants (e.g., EPE, DS-EVA, and DS-EPE modules), the intensity of the acetate group shows no changes before and after 1000 h of DH, as shown in Fig. S9. This confirms that failure due to acid corrosion is not the primary degradation mechanism.

3.1.6. *EQE analysis*

In addition, *EQE* and reflectance analyses were conducted on the modules before and after 1000 h of the DH test. A general minor decrease in the spectral response of *EQE* from 400 to 1200 nm was observed for the modules encapsulated with DS-EVA and DS-EPE, as shown in Fig. 7. This was due to a slight increase in light absorption of the encapsulants after the DH test, as shown in Fig. S10. Moreover, an apparent decrease in *EQE* and a slight decrease in reflectance in the short-wavelength range (280–400 nm) were also observed for these two types of modules, which is attributed to a deterioration in the UV-

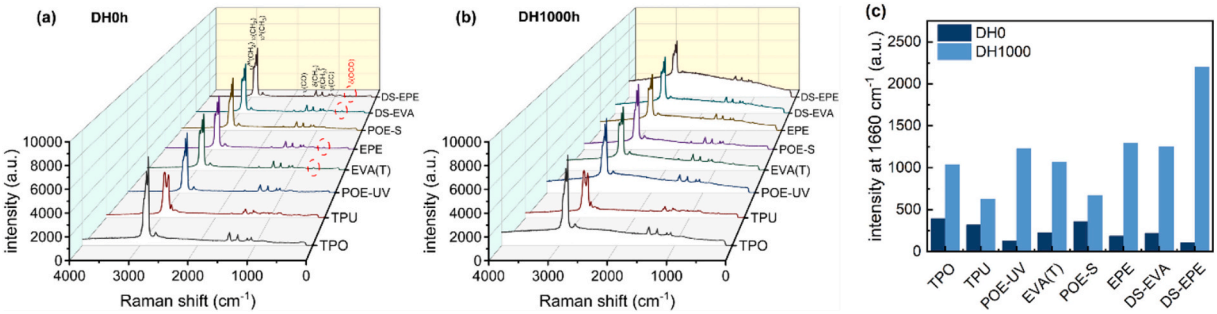

Fig. 6. Raw Raman spectra of encapsulant samples (a) before and (b) after 1000 h of the DH test. (c) Fluorescence background intensity of the modules at 1660 cm^{-1} before and after 1000 h of the DH test.

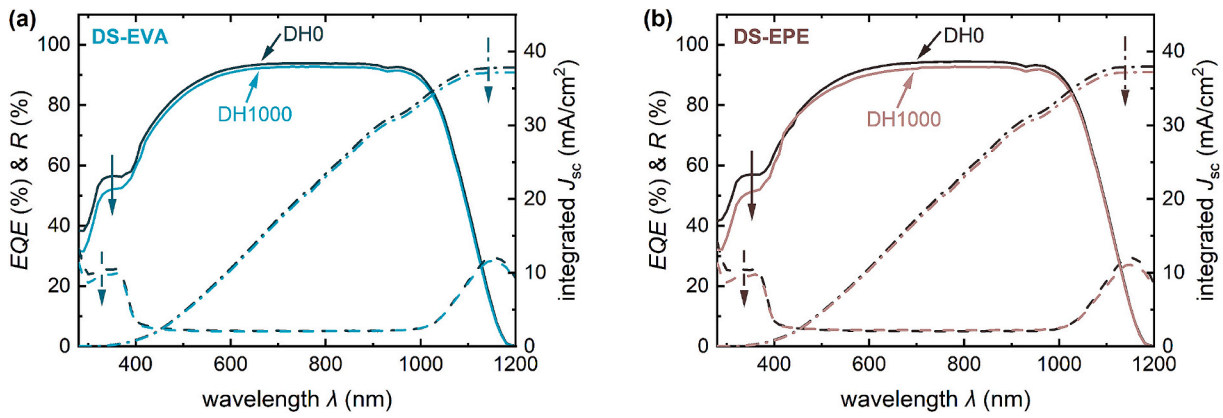

Fig. 7. *EQE* (solid line), reflectance (dash line) and integrated short-circuit current density (J_{sc}) (dash dot line) of modules encapsulated with downshifting encapsulants, (a) DS-EVA and (b) DS-EPE, before and after 1000 h of the DH test.

downshifting effect and/or an increase in the light absorption. Overall, the photocurrent losses due to the changes in optical properties of the encapsulants were 1.72 $\%_{rel}$ for the DS-EVA module and 1.98 $\%_{rel}$ for the DS-EPE module. The downshifting encapsulants shed light on protecting advanced cell technologies from UV degradation while simultaneously utilizing UV light. However, more attention should be paid not only to the UV stability but also to the DH stability of such new encapsulants when combined with unconventional module structures such as the lightweight solar module structures. Further investigation into its DH and UV stability is required.

A slight reduction in *EQE* from 280 to 500 nm was observed in the EVA module, as shown in Fig. S11(e). This reduction was attributed to the increased parasitic absorption of the EVA encapsulant after 1000 h DH, as discussed in 3.1.4. For the rest of the modules, we observed no obvious change in *EQE* and reflectance before and after DH, as shown in Fig. S11.

3.2. Improved damp heat stability of lightweight modules with different front sheets

The optimum combination of different encapsulants with SHJ solar cells within a lightweight module structure was determined in the above section. The lightweight module with TPO as the encapsulant, ETFE as the front sheet, and polyolefin-based foil with an aluminum interlayer as the back sheet showed the most damp-heat-stable performance, with only 3.22 $\%_{rel}$ efficiency degradation after 1000 h of the DH test compared with modules using other encapsulants. The efficiency degradation of such lightweight modules is even lower than the 5 $\%_{rel}$ required by IEC 61215 for glass modules. In order to further improve the damp heat stability of the lightweight modules, different front sheet materials were investigated in this section, including ETFE, PVF, PET/PVF laminated foil (denoted as PET1), and PET (denoted as PET2). The optical properties of the different front sheets were characterized by UV/vis spectroscopy. Fig. S12 shows the transmittance and reflectance of different front sheets. The ETFE has the highest transmittance and is also transmission to UV light. While PVF, PET1 and PET2 block UV light. Table 2 lists the configurations of the modules with different front sheets. All the modules used TPO as encapsulants. A polyolefin-based foil with an aluminum interlayer was used as the back sheet. The glass/glass and glass/back sheet modules were used as references for comparison.

3.2.1. Cell-to-module analysis

Fig. 8 shows the power density (module output power divided module weight) and area density (module weight divided module area) of the modules for each configuration. Lightweight modules have a lower area density while keeping a higher power density compared to conventional glass/glass and glass/back sheet modules, demonstrating their great potential for integrated PV applications.

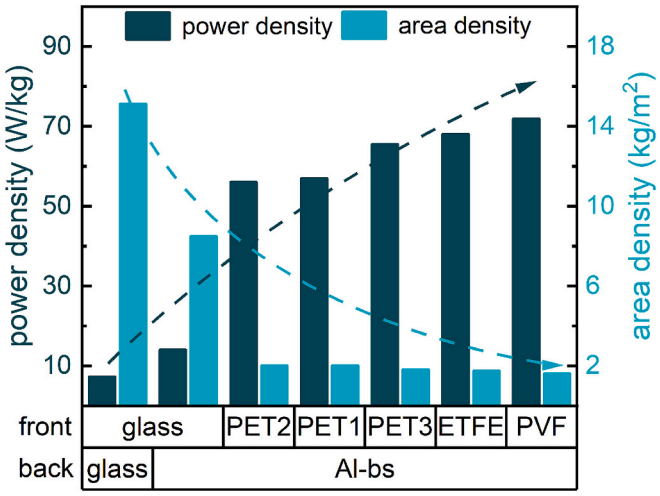

Fig. 8. Power density and area density of modules with different configurations.

Fig. 9 shows the efficiency loss from cell-to-module (CTM) for modules with different configurations. The CTM efficiency loss was calculated using the following equation:

$$CTM\ (\%) = \left(1 - \frac{Module\ Efficiency}{Cell\ Efficiency}\right) \times 100 \quad (3)$$

In general, the CTM efficiency loss is mainly attributed to the decrease in J_{sc} and the increase in R_s, as shown in Fig. S13. The CTM J_{sc} loss is related to the different optical properties of the different front sheets, as shown in Fig. S10 and the light absorption by the front side TPO encapsulant. The PET2 module had the lowest CTM efficiency due to its low J_{sc} loss and the small increase in R_s. However, the glass/glass module had the highest CTM J_{sc} loss. This is because the glass is also used as a back cover, which does not have the benefit of reflecting light from the rear side compared to other modules that use a white back sheet.

3.2.2. DH test results

Fig. 10 shows the development of the electrical properties of the modules with different front sheets after 1000 h of the DH test. The variance in efficiency for modules with the same configurations is shown in Fig. S14. It was found that replacing the ETFE with a PET2 front sheet reduced the module efficiency degradation from 3.22 $\%_{rel}$ to 0.47 $\%_{rel}$

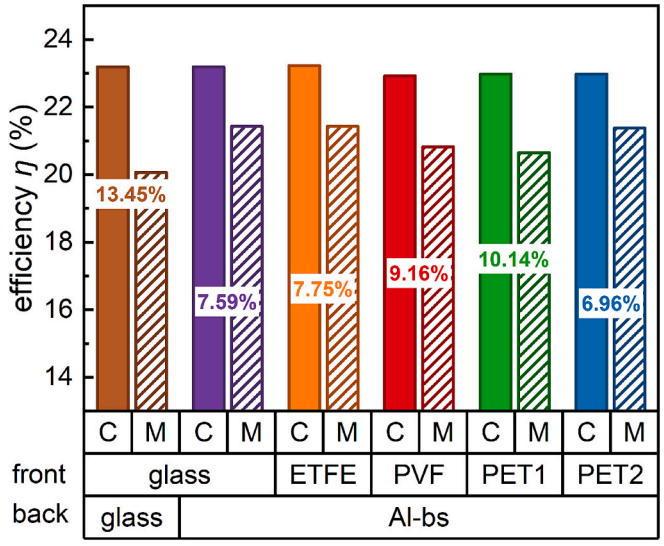

Fig. 9. Cell-to-module (CTM) efficiency loss of modules with different configurations. C stands for cell and M stands for module. The numbers in the graph indicate the CTM relative efficiency loss.

after 1000 h of DH. Its damp heat stability is the same as that of a traditional glass/back sheet module. We did not find any obvious defects in these modules after 1000 h of DH by visual inspection, as shown in Fig. S15 and the EL images, as shown in Fig. 11. The increase in R_s due to the damp heat effect was still the major cause of module efficiency degradation after 1000 h of the DH test.

3.2.3. *Equivalence between accelerated DH aging and field conditions*

The optimized lightweight SHJ solar modules demonstrate very promising performance and stability in accelerated DH aging test, performing as well as glass/back sheet modules. However, concerns have therefore been raised about their performance and reliability in the field conditions. Field test is important and imperative to understand the lifetime of lightweight SHJ solar modules in real-world conditions. Although field test provides a practical assessment of module degradation, it usually takes quite a long time before significant degradation can be observed. Therefore, accelerated aging tests are always performed to save time. However, investigation of the field performance and reliability of lightweight SHJ solar modules is beyond the scope of this work. Nevertheless, the acceleration factor (*AF*) modelling was proposed, which is instrumental in understanding the equivalence between accelerated aging test and field conditions [61,62].

The extent of module degradation under damp heat conditions primarily depends on temperature and humidity. The effect of these microclimatic factors, either individually or synergistically, on module degradation can be modelled using the Arrhenius equation, the modified Arrhenius equation, and the modified Peck's equation [61]. The Arrhenius model given by eq. (4) is the most commonly used model [61], which reveals the degradation rate as a function of temperature.

$$f(T) = A \bullet e^{\left(-\frac{E_a}{k_B T}\right)} \tag{4}$$

Where $f(T)$ is the DH aging rate of the modules that depends on temperature. k_B is the Boltzmann constant. E_a is the activation energy. A is a constant of the Arrhenius model.

Although the pristine Arrhenius model is widely applied to temperature-dominated reactions, however, it is insufficient for module degradation with regard to the effect of hydrolysis, since temperature alone cannot initiate the DHID. Relative humidity is another important factor causing degradation. To take this parameter into account, a modified Arrhenius equation, known as the Peck model [61,63,64], was proposed as shown in eq. (5).

$$f(T, RH) = A \bullet e^{\left(-\frac{E_a}{k_B T}\right)} \bullet (RH)^n \tag{5}$$

Then, the *AF* between the accelerated aging tests and the field conditions can be calculated by using eq. (6).

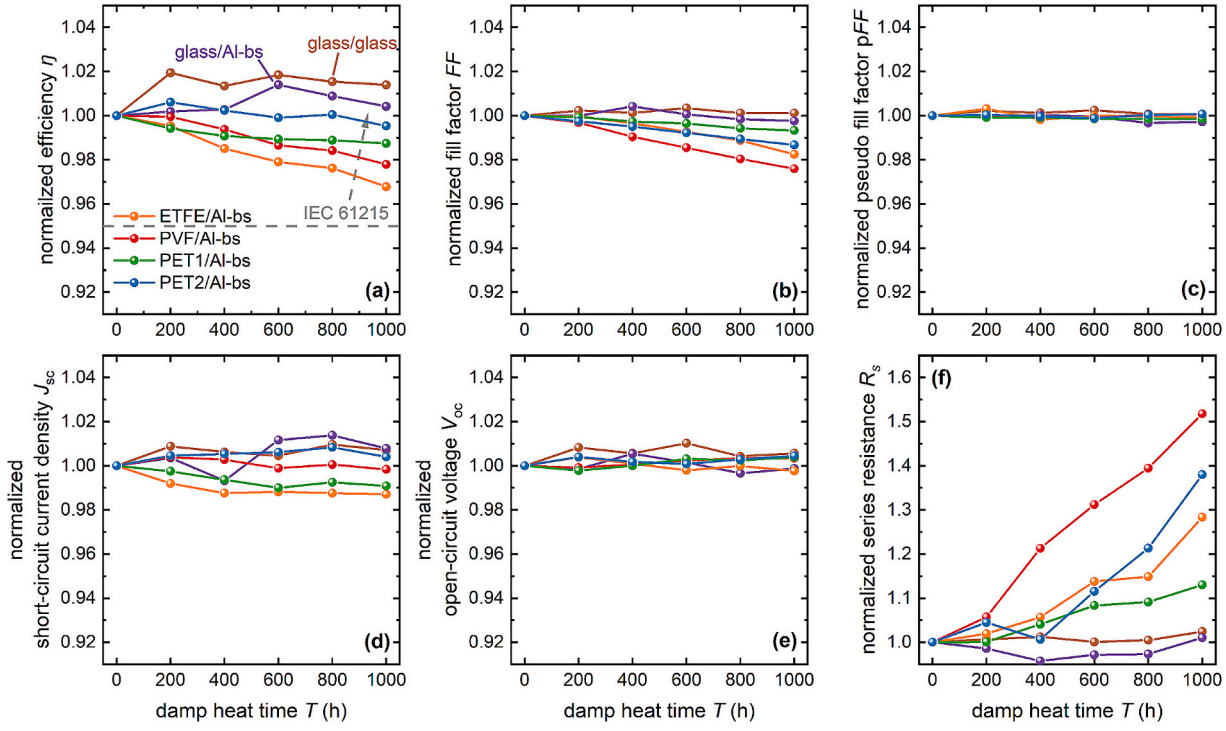

Fig. 10. Normalized values of (a) efficiency (η), (b) fill factor (*FF*), (c) pseudo fill factor (p*FF*), (d) short-circuit current density (J_{sc}), (e) open-circuit voltage (V_{oc}), and (f) series resistance (R_s) as a function of damp heat time for modules with different configurations.

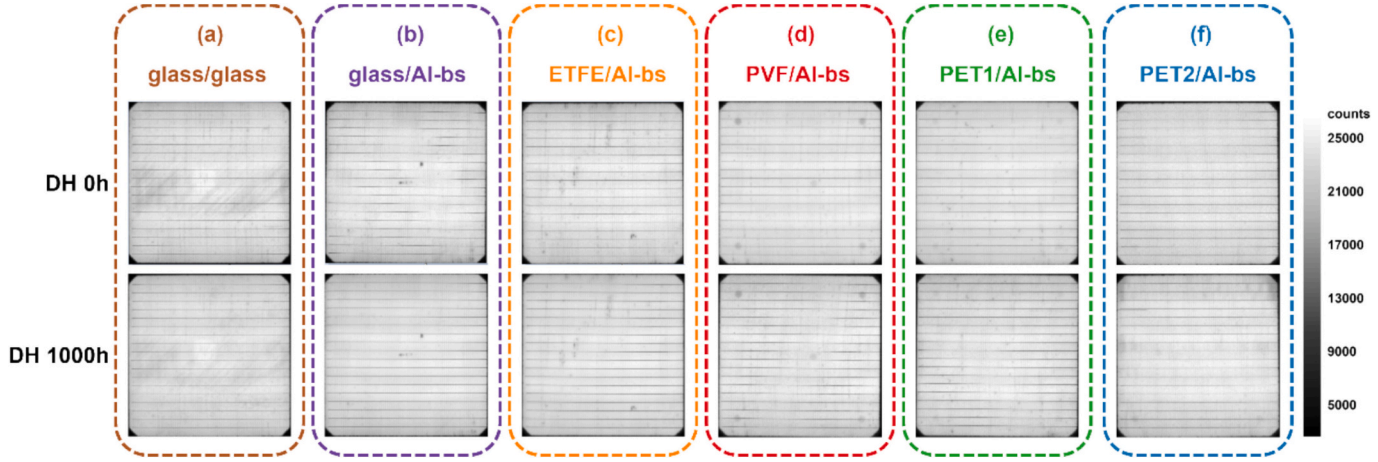

Fig. 11. EL images of modules with different configurations: (a) glass/glass, (b) glass/Al-bs, (c) ETFE/Al-bs, (d) PVF/Al-bs, (e) PET1/Al-bs, and (f) PET2/Al-bs before and after 1000 h of the DH test.

$$AF = \exp\left[\frac{E_a}{k_B}\left(\frac{1}{T_{module}} - \frac{1}{T_{test}}\right)\right] \bullet \left(\frac{RH_{test}}{RH_{field}}\right)^n \quad (6)$$

Where T_{module} is the module temperature in the field, which varies depending on the location and weather conditions, typically ranging from 25 to 75 °C [65]. T_{test} is the temperature of the DH test, which is 85 °C. RH_{field} is the relative humidity in the field, which also varies depending on the location and weather conditions. RH_{test} is the relative humidity during the DH test, which is 85 %. And n is the model parameter that indicates the impact of relative humidity on module degradation.

The determination of E_a is critical for modelling, as it depends not only on temperature, but also on the encapsulation material and the module configuration. Modules with different encapsulation materials result in different DH aging results. Essentially, a reliable estimate of E_a should be derived from experiments involving at least three temperature variations and linear degradation processes. Therefore, DH tests at three different temperature variations are required. However, so far, we have only conducted DH tests under two different temperature variation conditions: 85 °C, 85 % RH and 55 °C, 85 % RH. The normalized efficiencies of the modules during DH aging at 55 °C, 85 % RH conditions are shown in Fig. S16 in Supplementary Information. As expected, the modules demonstrate an even lower level of efficiency degradation at 55 °C, 85 % RH than at 85 °C, 85 % RH. Since the available data are insufficient to provide a reliable estimate of E_a and thus *AF*. Therefore, we will further investigate the equivalence between accelerated aging tests and field conditions in future work.

4. Conclusions

This study demonstrates the possibility of fabricating lightweight SHJ solar modules with a low area density (~ 2 kg/m^2) while preserving high power density (~ 70 W/kg) and damp heat stability even for single cell modules. For larger solar modules the power density is expected to be higher because of less cell interconnection material and less edge sealant material per area. We investigated the compatibility of different encapsulation materials with SHJ solar cells in lightweight module structures under damp heat conditions. A comprehensive analysis of the module degradation was performed focusing on the optical and electrical properties of the modules and chemical properties of the encapsulants. The results indicate that the efficiency loss in lightweight SHJ solar modules after DH test varied significantly, ranging from 3.22 %$_{\text{rel}}$ to 54.06 %$_{\text{rel}}$, depending strongly on the encapsulation materials. In general, an increase in R_s is the dominant cause of degradation of the module efficiency after 1000 h of the DH test. The module encapsulated with EPE showed the greatest efficiency degradation due to a significant increase in R_s. This can be attributed to two main factors: wires detaching from the ribbons due to solder joint failure and interconnection failure of wires detaching from the fingers. XCT revealed that the wires detached from the fingers, causing finger breakage, which is consistent with our observations from the EL images. EL imaging and Raman analysis revealed that metal corrosion was not the main degradation mechanism. An obvious yellowing effect was found in the EVA module after 1000 h of the DH test, but it only caused a negligible impact on the module performance. The TPO-encapsulated module was found to have the lowest degradation efficiency of 3.22 %$_{\text{rel}}$ after 1000 h of the DH test due to its low water permeability and high thermal stability compared to the other encapsulants investigated in this study. This indicated that TPO is a promising encapsulant for moisture-sensitive solar cells.

Furthermore, the optimized damp heat-stable lightweight solar module was successfully fabricated by using PET2 material instead of ETFE as the front sheet, polyolefin-based aluminum as the back sheet, and TPO as the encapsulant. The efficiency degradation of the module was only 0.47 %$_{\text{rel}}$ after 1000 h of the DH test. Its damp heat stability is the same as that of a traditional glass/back sheet module.

This study addressed the major challenge of DH stability for lightweight SHJ solar modules and could provide significant reference information for the development of damp heat-stable lightweight SHJ solar modules for industrial mass production. Nevertheless, thermo-mechanical properties are found to be another critical factor for lightweight solar modules when combining multilayer polymer foils with different thermo-mechanical properties. Further investigations in terms of the thermo-mechanical stability of the lightweight solar module will be investigated in our future work.

CRediT authorship contribution statement

Kai Zhang: Writing – original draft, Investigation, Data curation, Conceptualization. **Andreas Lambertz:** Writing – review & editing, Supervision, Project administration, Funding acquisition. **Krzysztof Dzięcioł:** Methodology, Investigation, Data curation. **Karsten Bittkau:** Writing – review & editing, Investigation. **Rongda Zhang:** Investigation. **Yanxin Liu:** Investigation. **Andreas Gerber:** Writing – review & editing, Resources. **Henrike Gattermann:** Writing – review & editing. **Rüdiger-A. Eichel:** Resources, Methodology. **Uwe Rau:** Writing – review & editing, Supervision. **Christoph J. Brabec:** Writing – review & editing. **Kaining Ding:** Writing – review & editing, Funding acquisition.

Declaration of competing interest

The authors declare that they have no known competing financial interests or personal relationships that could have appeared to influence the work reported in this paper.

Acknowledgements

The authors would like to thank Thomas Birrenbach, Niklas Bongartz, Volker Lauterbach, Christoph Zahren and Wilfried Reetz for their technical assistance. This work was supported by the Light.P.Roof project, which was funded by the Federal State North Rhine-Westphalia within the program "EFRE/JTF-Program NRW 2021-2027" under the grant number EFRE-20400082. Kai Zhang is grateful for the financial support from China Scholarship Council (No. 202108440128).

Appendix A. Supplementary data

Supplementary data to this article can be found online at https://doi.org/10.1016/j.apenergy.2025.126570.

Data availability

Data will be made available on request.

References

[1] Oliveira McCd, Diniz Cardoso ASA, Viana MM, Lins VdFC. The causes and effects of degradation of encapsulant ethylene vinyl acetate copolymer (EVA) in crystalline silicon photovoltaic modules: a review. Renew Sustain Energy Rev 2018;81:2299–317.
[2] Omazic A, Oreski G, Halwachs M, Eder GC, Hirschl C, Neumaier L, et al. Relation between degradation of polymeric components in crystalline silicon PV module and climatic conditions: a literature review. Solar Energy Mater Solar Cells 2019;192:123–33.
[3] Martins AC, Chapuis V, Virtuani A, Ballif C. Robust glass-free lightweight photovoltaic modules with improved resistance to mechanical loads and impact. IEEE J Photovoltaics 2019;9:245–51.
[4] Martins AC, Chapuis V, Virtuani A, Li H-Y, Perret-Aebi L-E, Ballif C. Thermo-mechanical stability of lightweight glass-free photovoltaic modules based on a composite substrate. Solar Energy Mater Solar Cells 2018;187:82–90.
[5] Martins AC, Chapuis V, Sculati-Meillaud F, Virtuani A, Ballif C. Light and durable: composite structures for building-integrated photovoltaic modules. Prog Photovoltaics Res Appl 2018;26:718–29.
[6] Yamaguchi M, Masuda T, Araki K, Sato D, Lee KH, Kojima N, et al. Development of high-efficiency and low-cost solar cells for PV-powered vehicles application. Prog Photovoltaics Res Appl 2020;29:684–93.
[7] Gaume J. Solight: a new lightweight PV module complying IEC standards. In: 33rd Eur Photovolt Sol Energy Conf Exhib; 2017.
[8] Kajisa T, Miyauchi H, Mizuhara K, Hayashi K, Tokimitsu T, Inoue M, et al. Novel lighter weight crystalline silicon photovoltaic module using acrylic-film as a cover sheet. Jpn J Appl Phys 2014;53.
[9] Boulanger A, Gaume J, Quesnel F, Ruols P, Rouby F. Operasol: a light photovoltaic panel with integrated connectors. In: 33rd Eur Photovolt Sol Energy Conf Exhib; 2017.
[10] Oreski G, Halm A, Schenk V, Krumlacher W, Nussbaumer H. Investigation of effects due to encapsulation thickness reduction in light weight modules. In: 3rd Eur Photovolt Sol Energy Conf Exhib; 2017.
[11] Descoeudres A, Allebé C, Badel N, Barraud L, Champliaud Jonathan, Debrot F, et al. Silicon heterojunction solar cells: towards low-cost high-efficiency industrial devices and application to low-concentration PV. Energy Procedia 2015;77:508–14.
[12] Louwen A, van Sark W, Schropp R, Faaij A. A cost roadmap for silicon heterojunction solar cells. Solar Energy Mater Solar Cells 2016;147:295–314.
[13] Trinasolar. Trinasolar sets new n-type solar cell efficiency world record of 27.08%. 2017. https://static.trinasolar.com/en-apac/resources/newsroom/aptrinasolar-sets-new-n-type-solar-cell-efficiency-world-record-27082024.
[14] Liu W, Zhang L, Yang X, Shi J, Yan L, Xu L, et al. Damp-heat-stable, high-efficiency. Indust Size Silicon Heterojunction Solar Cells Joule 2020;4:913–27.
[15] Zhang K, Mashkov O, Yaqin Muhammad A, Doll B, Lambertz A, Bittkau K, et al. Damp-heat–induced degradation of lightweight silicon heterojunction solar modules with different transparent conductive oxide layers. Prog Photovoltaics Res Appl 2025;33:541-550.
[16] Peike C, Hadrich, I. W, Dürr I. Overview of PV module encapsulation materials Photovoltaics International 2013b;19:85–92.
[17] Oreski G, Omazic A, Eder GC, Voronko Y, Neumaier L, Mühleisen W, et al. Properties and degradation behaviour of polyolefin encapsulants for photovoltaic modules. Prog Photovoltaics Res Appl 2020;28:1277–88.
[18] Tracy J, D'Hooge DR, Bosco N, Delgado C, Dauskardt R. Evaluating and predicting molecular mechanisms of adhesive degradation during field and accelerated aging of photovoltaic modules. Prog Photovoltaics Res Appl 2018;26:981–93.
[19] Kempe M. Modeling of rates of moisture ingress into photovoltaic modules. Solar Energy Mater Solar Cells 2006;90:2720–38.
[20] Bai Y, Zhao Y, Li J, Chen H, Lambertz A, Qiu Q, et al. Lower levelized cost of energy achievement of silicon heterojunction solar modules with low water vapor transmission rate encapsulants. Energ Technol 2023:11.
[21] Lisco F, Bukhari F, Jones LO, Law AM, Walls JM, Ballif C. ETFE and its role in the fabrication of lightweight c-Si solar modules. IEEE J Photovoltaics 2023;13:349–54.
[22] Luo B, Govaerts J, Lisco F, Eder G, Breukers B, Ruttens B, et al. Encapsulation strategies for mechanical impact and damp heat reliability improvement of lightweight photovoltaic modules towards vehicle-integrated applications. Solar Energy Mater Solar Cells 2024;273.
[23] Czanderna AW, Pern FJ. Encapsulation of PV modules using ethylene vinyl acetate copolymer as a pottant: a critical review. Solar Energy Mater Solar Cells 1995;43:101–81.
[24] Bosco N, Moffitt S, Schelhas LT. Mechanisms of adhesion degradation at the photovoltiac module's cell metallization-encapsulant interface. Prog Photovoltaics Res Appl 2019;27:340–5.
[25] Han C. Analysis of moisture-induced degradation of thin-film photovoltaic module. Solar Energy Mater Solar Cells 2020;210.
[26] Jankovec M, Annigoni E, Ballif C, Topič M. In-situ determination of moisture diffusion properties of PV module encapsulants using digital humidity sensors. In: 2018 IEEE 7th World Conference on Photovoltaic Energy Conversion, WCPEC 2018 - A Joint Conference of 45th IEEE PVSC, 28th PVSEC and 34th EU PVSEC; 2018. p. 415–7.
[27] Segbefia OK, Imenes AG, Sætre TO. Moisture ingress in photovoltaic modules: a review. Solar Energy 2021;224:889–906.
[28] Novoa FD, Miller DC, Dauskardt RH. Environmental mechanisms of debonding in photovoltaic backsheets. Solar Energy Mater Solar Cells 2014;120:87–93.
[29] Novoa FD, Miller DC, Dauskardt RH. Adhesion and debonding kinetics of photovoltaic encapsulation in moist environments. Prog Photovoltaics Res Appl 2016;24:183–94.
[30] Ballif C, Li H-Y, Annigoni E, Galliano F, Escarré J, Meillaud F, et al. Impact of moisture ingress in PV modules on long-term performance: the role of EVA formulation, module design and climate. IEEE Photovoltaics 2014:1545–51.
[31] Wohlgemuth JH, Kempe MD. Equating Damp Heat Testing with Field Failures of PV Modules. 2013 IEEE 39th Photovoltaic Specialists Conference (PVSC). 2013. p. 0126–31.
[32] Eder GC, Voronko Y, Dimitriadis S, Knöbl K, Újvári G, Berger KA, et al. Climate specific accelerated ageing tests and evaluation of ageing induced electrical, physical, and chemical changes. Prog Photovoltaics Res Appl 2018;27:934–49.
[33] Kempe MD, Jorgensen GJ, Terwilliger KM, McMahon TJ, Kennedy CE, Borek TT. Acetic acid production and glass transition concerns with ethylene-vinyl acetate used in photovoltaic devices. Solar Energy Mater Solar Cells 2007;91:315–29.
[34] Hu Y, French RH. Durability and reliability of polymers and other materials in photovoltaic modules. William Andrew Publishing; 2019.
[35] Peshek TJ, Fada JS, Martin IT. Durability and reliability of polymers and other materials in photovoltaic modules. William Andrew Publishing; 2019.
[36] Hoffmann S, Koehl M. Effect of humidity and temperature on the potential-induced degradation. Prog Photovoltaics Res Appl 2014;22:173–9.
[37] Hülsmann P, Weiß KA, Köhl M. Temperature-dependent water vapour and oxygen permeation through different polymeric materials used in photovoltaic-modules. Prog Photovoltaics Res Appl 2012;22:415–21.
[38] Yang HE. Durability and reliability of polymers and other materials in photovoltaic modules. William Andrew Publishing; 2019.
[39] Mon G, Wen L, Ross Jr RG, Adent D. Effects of temperature and moisture on module leakage currents. In: 18th IEEE photovoltaic specialists conference. Las Vegas; 1985. p. 1179–85.
[40] Oreski G, Wallner GM. Aging mechanisms of polymeric films for PV encapsulation. Solar Energy 2005;79:612–7.
[41] Yang C, Xing X, Li Z, Zhang S. A comprehensive review on water diffusion in polymers focusing on the polymer-metal Interface combination. Polymers (Basel) 2020:12.
[42] Peike C, Hoffmann S, Hülsmann P, Thaidigsmann B, Weiß KA, Koehl M, et al. Origin of damp-heat induced cell degradation. Solar Energy Mater Solar Cells 2013;116:49–54.
[43] La Mantia FP, Malatesta V, Ceraulo M, Mistretta MC, Koci P. Photooxidation and photostabilization of EVA and cross-linked EVA. Polymer Testing 2016;51:6–12.
[44] Hasan O, Arif AFM. Performance and life prediction model for photovoltaic modules: effect of encapsulant constitutive behavior. Solar Energy Mater Solar Cells 2014;122:75–87.
[45] McIntosh KR, Powell NE, Norris AW, Cotsell JN, Ketola BM. The effect of damp-heat and UV aging tests on the optical properties of silicone and EVA encapsulants. Prog Photovoltaics Res Appl 2011;19:294–300.
[46] Sinha A, Qian J, Moffitt SL, Hurst K, Terwilliger K, Miller DC, et al. UV-induced degradation of high-efficiency silicon PV modules with different cell architectures. Prog Photovoltaics Res Appl 2022;31:36–51.
[47] Commission IE. IEC 61215–2: Terrestrial photovoltaic (PV) modules-design qualification and type approval-part 2: Test procedures. 2021.
[48] Wenham SR, Green MA, Watt ME, Corkish R, Sproul A. Applied photovoltaics. 3rd ed. London: Routledge; 2011.

[49] Spataru SV, Sera D, Hacke P, Kerekes T, Teodorescu R. Fault identification in crystalline silicon PV modules by complementary analysis of the light and dark current–voltage characteristics. Prog Photovoltaics Res Appl 2015;24:517–32.
[50] Altermatt PP, Heiser G, Aberle AG, Wang A, Zhao J, Robinson SJ, et al. Spatially resolved analysis and minimization of resistive losses in high-efficiency Si solar cells. Prog Photovoltaics Res Appl 1996;4:399–414.
[51] Vandewal K, Tvingstedt K, Gadisa A, Inganas O, Manca JV. On the origin of the open-circuit voltage of polymer-fullerene solar cells. Nat Mater 2009;8:904–9.
[52] Würfel P. Physics of solar cells from principles to new concepts. WILEY-VCH Verlag GmbH & Co. KGaA; 2005.
[53] Aghaei M, Fairbrother A, Gok A, Ahmad S, Kazim S, Lobato K, et al. Review of degradation and failure phenomena in photovoltaic modules. Renew Sustain Energy Rev 2022;159.
[54] Yu J, Bai Y, Qiu Q, Sun Z, Ye L, Qian C, et al. Reliability of transparent conductive oxide in ambient acid and implications for silicon solar cells. eScience 2024:4.
[55] Kempe MD, Dameron AA, Reese MO. Evaluation of moisture ingress from the perimeter of photovoltaic modules. Prog Photovoltaics Res Appl 2013;22:1159–71.
[56] Li G, Akram MW, Jin Y, Chen X, Zhu C, Ahmad A, et al. Thermo-mechanical behavior assessment of smart wire connected and busbarPV modules during production, transportation, and subsequent field loading stages. Energy 2019;168:931–45.
[57] Zarmai MT, Ekere NN, Oduoza CF, Amalu EH. Evaluation of thermo-mechanical damage and fatigue life of solar cell solder interconnections. Robotics Comp Integr Manuf 2017;47:37–43.
[58] Oreski G, Wallner GM. Evaluation of the aging behavior of ethylene copolymer films for solar applications under accelerated weathering conditions. Solar Energy 2009;83:1040–7.
[59] Koenig JL. Raman scattering of synthetic polymers-a review. Appl Spectrosc Rev 1971;4:233–305.
[60] Peike C, Kaltenbach T, Weiß KA, Koehl M. Non-destructive degradation analysis of encapsulants in PV modules by Raman spectroscopy. Solar Energy Mater Solar Cells 2011;95:1686–93.
[61] Sinha A, Gopalakrishna H, Bala Subramaniyan A, Jain D, Oh J, Jordan D, et al. Prediction of climate-specific degradation rate for photovoltaic Encapsulant discoloration. IEEE J Photovoltaics 2020;10:1093–101.
[62] DDaO Haillant. Environmental durability of PV modules - a model for accelerated testing. In: 37th IEEE photovoltaic specialists conference. Seattle, WA, USA: IEEE; 2011. p. 000091–5.
[63] Hallberg Ö, Peck DS. Recent humidity accelerations, a base for testing standards. Qual Reliability Eng Int 1991;7:169–80.
[64] Ren J, Zhao W, Shi J, Yan Z, Chen S, Luo Y, et al. Predicting the lifetime of HJT modules towards the outdoor real-world environment. Solar Energy Mater Solar Cells 2024;272.
[65] Li X, Yang Y, Huang S, Jiang K, Li Z, Zhao W, et al. Reassessment of silicon heterojunction cell performance under operating conditions. Solar Energy Mater Solar Cells 2022;247.